PNAS
www.pnas.org

Supplementary Information for

Cortical circuit activity underlying sleep slow oscillations and spindles

Niels Niethard[1*], Hong-Viet V. Ngo[1,2], Ingrid Ehrlich[3,4,5], Jan Born[1,3*]

[1] Institute of Medical Psychology and Behavioral Neurobiology, University of Tübingen, 72076 Tübingen, Germany.
[2] School of Psychology, University of Birmingham, B15 2TT Birmingham, United Kingdom.
[3] Center for Integrative Neuroscience, University of Tübingen, 72076 Tübingen, Germany.
[4] Hertie Institute for Clinical Brain Research, University of Tübingen, 72076, Germany
[5] IBBS, Dept. of Neurobiology, University of Stuttgart, 70569 Stuttgart, Germany

Email: niels.niethard@uni-tuebingen.de or jan.born@uni-tuebingen.de

This PDF file includes:

www.pnas.org/cgi/doi/10.1073/pnas.1805517115

Supplementary Information Text

Surgery. The mice were implanted with a headpost for subsequent experimentation. They were anesthetized with 0.1 mg/g ketamine and 0.008 mg/g xylazine with a supplement of isoflurane. Dexamethasone (0.08 mg) was sometimes administered to reduce tissue swelling. Lidocaine was applied to the wound margins for topical anesthesia. A custom-built headpost was glued to the skull and subsequently cemented with dental acrylic (Lang Dental, U.S.A.).

The headpost implantation was followed by virus injection and window implantation. For two-photon experiments, a craniotomy of 1.2 x 2.0 mm was made above the sensorimotor cortex (1.1 mm caudal and 1.0-1.3 mm lateral from the bregma). In the area of the craniotomy, two viruses were injected (AAV2/1-syn-GCaMP6f and AAV2/1-flex-tdTomato) at a depth of 130-300 μm below the dura. Control animals were injected with one virus only (AAV1.CB7.CI.eGFP.WPRE.rBG) to express calcium-independent green fluorescent protein (GFP). For wide-field imaging experiments, the craniotomy was larger (8 mm x 9 mm) and covered the whole dorsal cortex (Fig. 4). Two layers of coverglasses (size depending on the area of craniotomy) were implanted as an imaging window. The space between the imaging window and the skull was sealed with 1.5 - 2 % agarose, and the window was cemented with dental acrylic.

Electrodes for electroencephalographic (EEG) recordings in the two-photon experiments were implanted contralateral to the imaging window. The skull was exposed and two bone screws (PlasticOne, U.S.A.) were implanted (frontal electrode: anterior +1.5 mm, lateral 1.5 mm; parietal electrode: posterior -1.5 mm, lateral 2.5 mm from bregma). A silver wire (Science Products, Germany) implanted on the brain surface (posterior 1 mm, lateral 0 mm from lambda) served as reference. For wide-field imaging experiments, four silver wires (Science Products, Germany) were implanted between the dura mater and the imaging window (Fig. 4), two in the anterior region of the imaging window (anterior +1.5 mm, lateral 1.5 mm; from bregma) and two in occipital regions (anterior -3 mm, lateral 1.5 mm; from bregma). For electromyographic (EMG) recordings, in all experiments two stainless steel wires (Science Products, Germany) were implanted into the neck muscle. After surgery the animals were single-housed in their home cages and calcium imaging was conducted after at least 10 days of recovery.

Head fixation procedure. After handling for 10 min per day for one week, the animals were habituated to the head-fixation. Habituation consisted of 4 sessions per day for one week with increasing fixation durations (30 s, 3 min, 10 min, 30 min) interleaved by 10-min resting intervals. Habituation was conducted until the day prior to the first imaging session during the early light phase.

EEG and EMG recordings. Sleep stages were identified based on EEG and EMG recordings during the imaging sessions. EEG and EMG signals were amplified, filtered (EEG: 0.01 – 300 Hz; EMG: 30 – 300 Hz) and sampled at a rate of 1000 Hz (amplifier: Model 15A54, Grass Technologies, U.S.A.). Based on EEG/EMG signals for succeeding 10-s epochs, the brain state of the mouse was classified into Wake, Slow wave sleep (SWS), and Rapid Eye Movement (REM) sleep stages (1,2). Sleep stage identification was supported using the software SleepSign for animals (Kissei Comtech, Japan).

Offline detection of sleep slow oscillations and spindles. To detect discrete slow oscillation events during SWS, offline algorithms were adopted from previously described procedures (3-5). In brief, the EEG was bandpass filtered between 0.2 - 4.5 Hz and then, all positive-to-negative zero crossings of the signal as well as the local minimum and maximum between each two successive crossings were marked. Intervals between two succeeding positive-to-negative zero-crossings were identified as a slow oscillation event when the length of this interval was between 0.4 - 2 s and when the minimum amplitude and minimum-to-maximum amplitude was greater than 66.6 % of the average of the respective amplitude values across the whole recording. For these remaining events the enclosing zero-crossings represent the onset and end of the corresponding slow oscillation cycle.

For analyses, identified SO events were averaged time locked to the negative-half wave peak (0 s). The analyses of concurrent calcium activity concentrated on a window from -2 to +3 s around the negative SO halfwave peak. This window was wide enough to also cover SO events with upstates of longer duration and has been similarly used in previous studies (5 - 7). Averaging was time-locked to the negative half-wave peak of the SO (reflecting the downstate maximum) because it represents the temporally most distinct event during the SO and, thus, allows for optimally estimating the beginning and end of processes of interest, associated with the SO up- and down states, respectively. Previous studies comparing SO averaging time-locked the negative versus positive half-wave peaks of the SO revealed that time-locking to the positive half-wave peak (i.e., upstate) does not only result in a more smeared average SO waveform (with lower amplitude). Also, the increase in spindle activity occurring phase-locked to the SO upstate was distinctly reduced with phase-locking of the signal to the positive half-wave peak (8), which reflects that the positive half-wave peak provides only an imprecise time reference for averaging SO-related signals.

Detection of discrete spindles was performed following an algorithm described by (9). The EEG signal was band pass filtered between 7 - 15 Hz, rectified and, subsequently, all maxima were interpolated to yield the envelope for this frequency band. A spindle event was identified whenever the envelope exceeded an individual threshold for a duration of 0.5 to 3.0 s, whereby the threshold was defined by the standard deviation of the filtered signal during all SWS epochs of an individual mouse multiplied by a factor of 1.5. Thus, the positive and subsequent negative threshold crossing represented the onset and end of a spindle event. Detected spindle events were then characterized by their onset. For analyses, the root mean square signal (RMS) during identified spindle events was averaged time-locked to the spindle onset. The analyses of accompanying calcium signal centered – as for SO events – on an interval -2 to +3 s around the spindle event.

The same procedure was applied to separately identify slow and fast spindles, after pre-filtering the EEG signal in the respective 7 - 11 Hz and 11 - 15 Hz bands.

In subsequent analyses the calcium signal was analyzed for three different EEG events: (i) solitary slow oscillations that occurred in the absence of a spindle during the slow oscillation-cycle and in a 250-ms interval before and after the cycle, (ii) solitary spindles that occurred without any overlap with an identified slow oscillation-event, and (iii) slow oscillation-spindle events defined by slow oscillation-events where a spindle nested in the slow oscillation-upstate. Specifically, spindle onset occurred in the interval between slow oscillation-onset and the positive slow oscillation half-wave peak + 250 ms. Also, there were no spindles in the 250-ms interval preceding the slow oscillation-spindle event.

Immunohistochemistry. Immunostaining was performed using standard procedures. Following experiments, mice were deeply anesthetized (0.3 mg/g ketamine and 0.024 mg/g xylazine, i.p.) and intracardially perfused with 4 % paraformaldehyde in 0.1 M phosphate buffered saline (4 % PFA). The brains were removed from the skull, post-fixed in 4 % PFA at 4 °C overnight, and rinsed 3 x with 0.1 M phosphate buffered saline (PBS). Coronal slices (thickness 65 µm) were cut using a vibratome and blocked in 10 % normal goat serum (NGS, Jackson ImmnunoResearch, West Grove, U.S.A) and 0.3 % Triton X-100 (Sigma-Aldrich, Buchs, Switzerland) in 0.1 M PBS for 1.5 h at room temperature. Slices were incubated with anti-PV rabbit primary antibody (1:1000; #24428, Immunostar, U.S.A., RRID: AB_572259) or anti-SOM rabbit primary antibody (1:1000; #T-4547, Peninsula Laboratories, U.S.A., RRID AB_518618) in carrier solution (2% NGS and 0.3% Triton in PBS) for 48 h at 4 °C. After 4 x 10 min rinses with 0.1 M PBS sections were incubated in goat anti-Rabbit IgG antibodies conjugated either with Alexa 405 (for PV staining, AB_221605) or Alexa 633 (for SOM staining, AB2535732) (both from Thermo Fisher Scientific, 1:1000) in carrier solution for 3 h at room temperature on the shaker. After washing in 0.1 M PBS, slices were mounted on slides for imaging. Images were acquired on a confocal microscope (LSM 710, Carl Zeiss, Germany) with a 40x 1.3 NA oil-immersion objective. The frame size was 1024 x 1024 pixels and the z-resolution was set to one airy unit. The following laser lines were used: 488 nm (GCaMP6f) 561 nm (tdTomato), and 405 or 633 nm (for detection of PV or SOM secondary antibodies). To ensure co-labeling of PV-In and SOM-In with tdtomato and GCamp6f each imaging area was manually chosen before the actual recording session started, thus maximizing the number of cells expressing both tdtomato and GCamp6f. Overall, the fraction of cells only expressing tdtomato but not GCamp6f for PV-In and SOM-In was below 2%.

Two-photon imaging. *In vivo* imaging was performed as described previously (10): A two-photon microscope was used based on the MOM system (Sutter, U.S.A) controlled by ScanImage software (11). The light source was a pulsed Ti:sapphire laser (λ = 980 nm; Chameleon, Coherent, U.S.A.). Red and green fluorescence photons were collected with an objective lens (Nikon, 16x, 0.80 NA, Japan), separated by a 565 nm dichroic mirror (Chroma, 565dcxr, U.S.A.) and barrier filters (green: ET525/70m-2p, red: ET605/70m-2p), and measured using photomultiplier tubes (Hamamatsu Photonics,

H10770PA-40, Japan). The imaging frame consisted of 1024 x 256 pixels, and the frame rate was 5.92 Hz (169 ms per frame). Images were collected from neurons in layer 2/3 at a depth of 150-250 µm.

Wide-field imaging. For wide-field calcium imaging, a CCD camera (iXon X3 888, Andor Technology, U.S.A.) was focused on the cortical surface using a macroscope (MVX-10, Olympus, Japan). The illumination light sources were 470 nm light emitting diodes (Thorlabs, U.S.A.). The filter cube contained an excitation bandpass filter of 470/40 nm, a dichroic filter of 495 nm, and an emission bandpass filter of 525/50 nm. The zoom was adjusted to cover the entire window. The imaging frame consisted of 125 x 125 pixels, and the frame rate was 48.86 – 56.26 Hz (17.8 – 20.5 ms per frame). The precise timing of individual frames was saved as voltage pulse in the EEG recording system.

Principal component analysis (PCA). PCA was used to further explore the temporal dynamics in calcium activity for the three different cell types during solitary slow oscillations and solitary spindles. Analyses were run in Matlab (functions: "pca" and "rotatefactors"). We performed two separate PCAs on the ΔF/F signals during the 2s to +3 s windows around the EEG slow oscillations (0 s referring to the negative half-wave peak of the individual events) and spindles (0 s referring to the individual spindle onset). PCAs revealed three main components, which explained 63.05 % (solitary slow oscillations) and 63.3 % (solitary spindles) of the total variance. We, then, compared the varimax rotated component scores only for the component showing highest (positive or negative) factor loadings during the oscillatory event of interest between the three different cell types using ANOVA with subsequent *t*-tests.

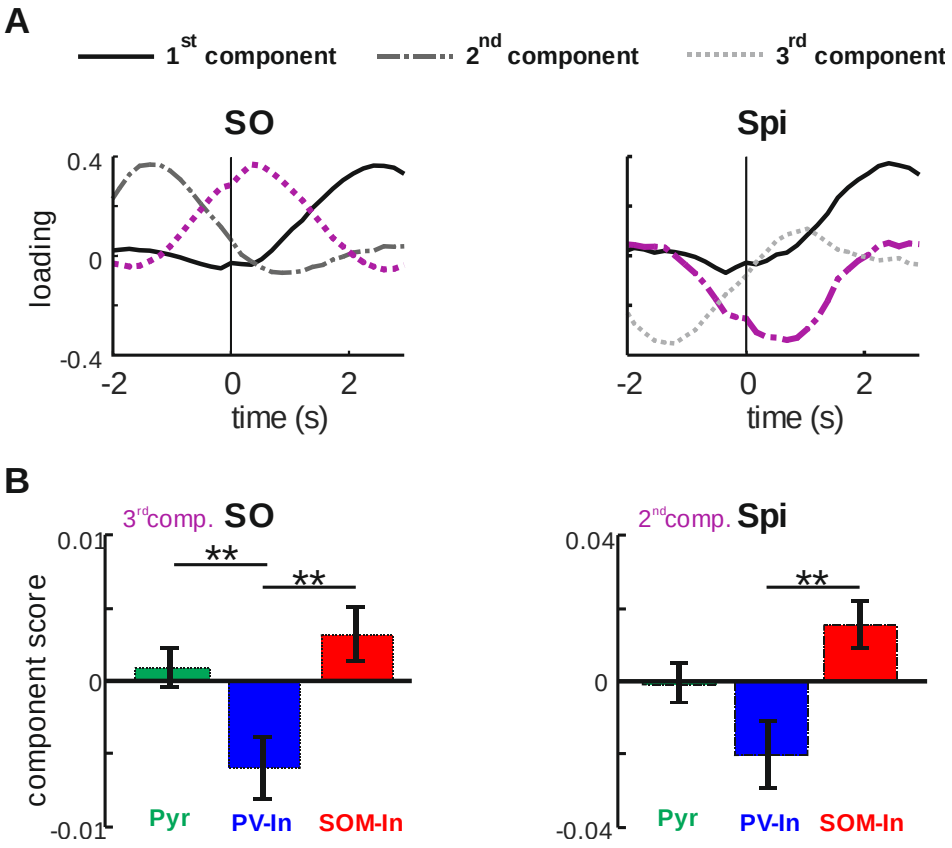

Fig. S1. Principal components of calcium activity during slow oscillations and spindles discriminate PV-In and SOM-In activity. (*A*) Component loadings for the first three varimax rotated components of calcium activity during solitary slow oscillations (SO), time-locked to the negative half-wave peak (0 s) and during solitary spindles (Spi), time-locked to the spindle onset. Components used for analysis shown in B are in violet. For SOs, this is the 3nd extracted component showing high positive loadings in a window covering both the downstate and upstate of the SO. For spindles, this is the 2nd component with high negative loadings reaching maximum values around the spindle maximum. (*B*) Mean (± SEM) component scores for the components showing highest (absolute) loadings around the reference time point (0 s) for solitary SOs (left) and solitary spindles (right) for putative Pyr (green), PV-In (blue) and SOM-In (red) cells. ** $P < 0.01$ for pairwise comparisons between cell types. Note: PV-In and SOM-In show opposing scores during slow oscillations and spindles, reflecting predominant activity of SOM-In over PV-in the course of SOs but - because of the negative loadings of the respective component during this time - predominant PV-In over SOM-In activity in the course of spindles.

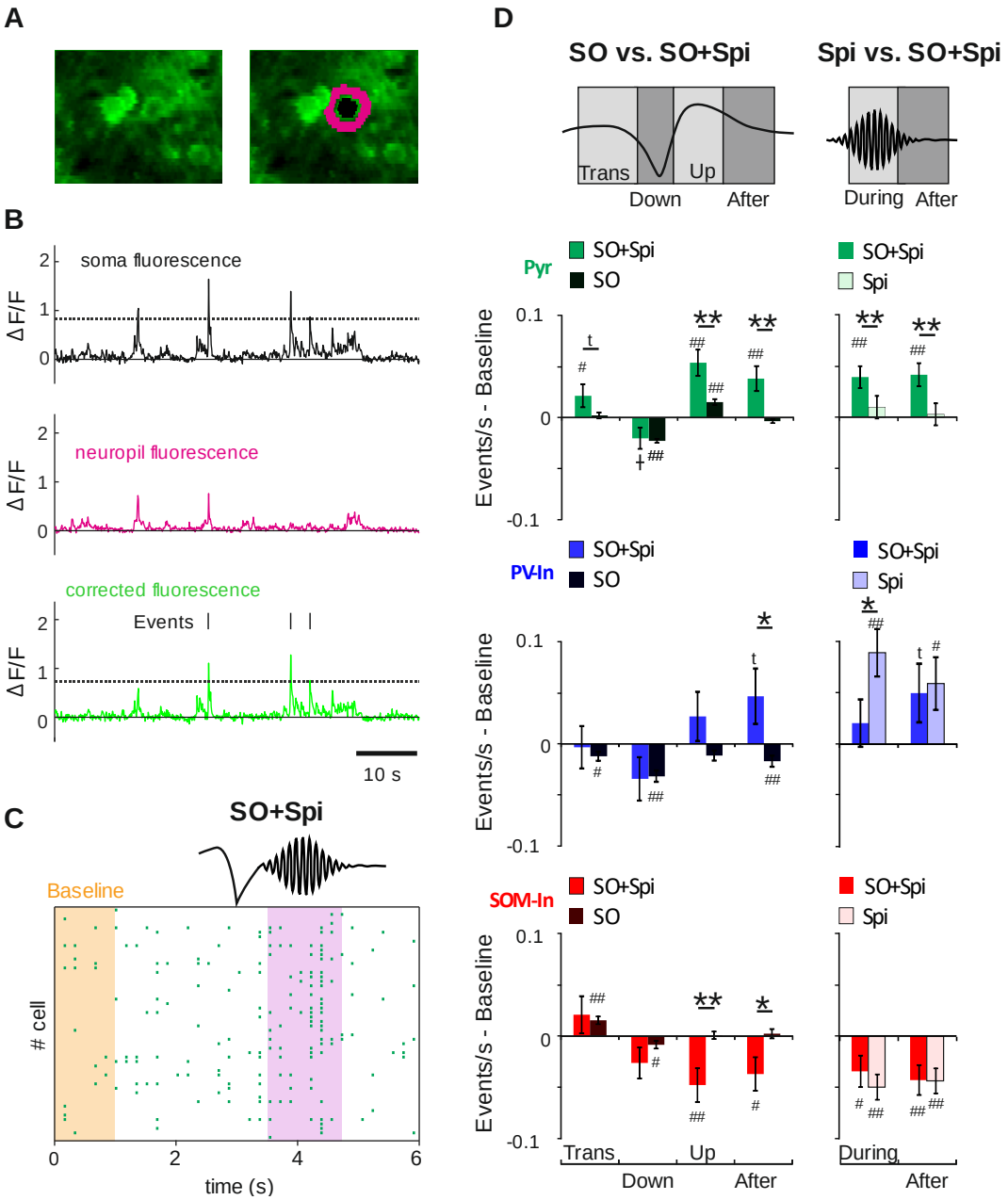

Fig. S2. Neuropil correction of ΔF/F signal. (*A*) Illustration of the area defined for neuropil fluorescence correction. The donut-shaped neuropil area (pink) was defined as a circle (three pixel radius) around each cell's ROI (black) omitting soma from other cells and the pixels directly adjoining the cell's soma. (*B*) Example ΔF/F signal traces from the cell shown in *A*, (top) from the soma, (middle) from the neuropil area, and (bottom), the corrected ΔF/F signal after subtracting 0.7 x neuropil ΔF/F. The dotted horizontal line represents the threshold (two standard deviations above the median of the corrected signal) used for event detection. (*C*) Example raster plot showing activity from putative pyramidal cells (Pyr) being active during a six second

example interval including a slow oscillation-spindle event (SO + Spi). Yellow shaded area indicates the interval used to measure baseline activity; right violet shaded area indicates Up interval of the slow oscillation covering the spindle (with high event rates). (*D*) Left: Comparison of mean (± SEM) event rates (per second) between solitary SO and SO + Spi events for the positive-to-negative Transition phase (Trans, -0.32 to -0.00 s, with reference to SO negative half-wave peak = 0 s), the Down phase (-0.00 to 0.16 s), the Up phase (0.32 to 0.48 s) and the following After phase (0.54 to 3 s). Right: Comparisons between mean (± SEM) event rates between solitary spindles and SO + Spi events for the phase During the acute spindle (0 to 1 s with reference to spindle onset set to 0 s) and the After phase (1 to 3 s). ** $P < 0.01$, * $P < 0.05$, t $P < 0.1$ for pairwise comparisons between solitary events and SO + Spi events respectively. ## $P < 0.01$, # $P < 0.05$, t $P < 0.1$, for difference from baseline activity (-3 to -2 s).

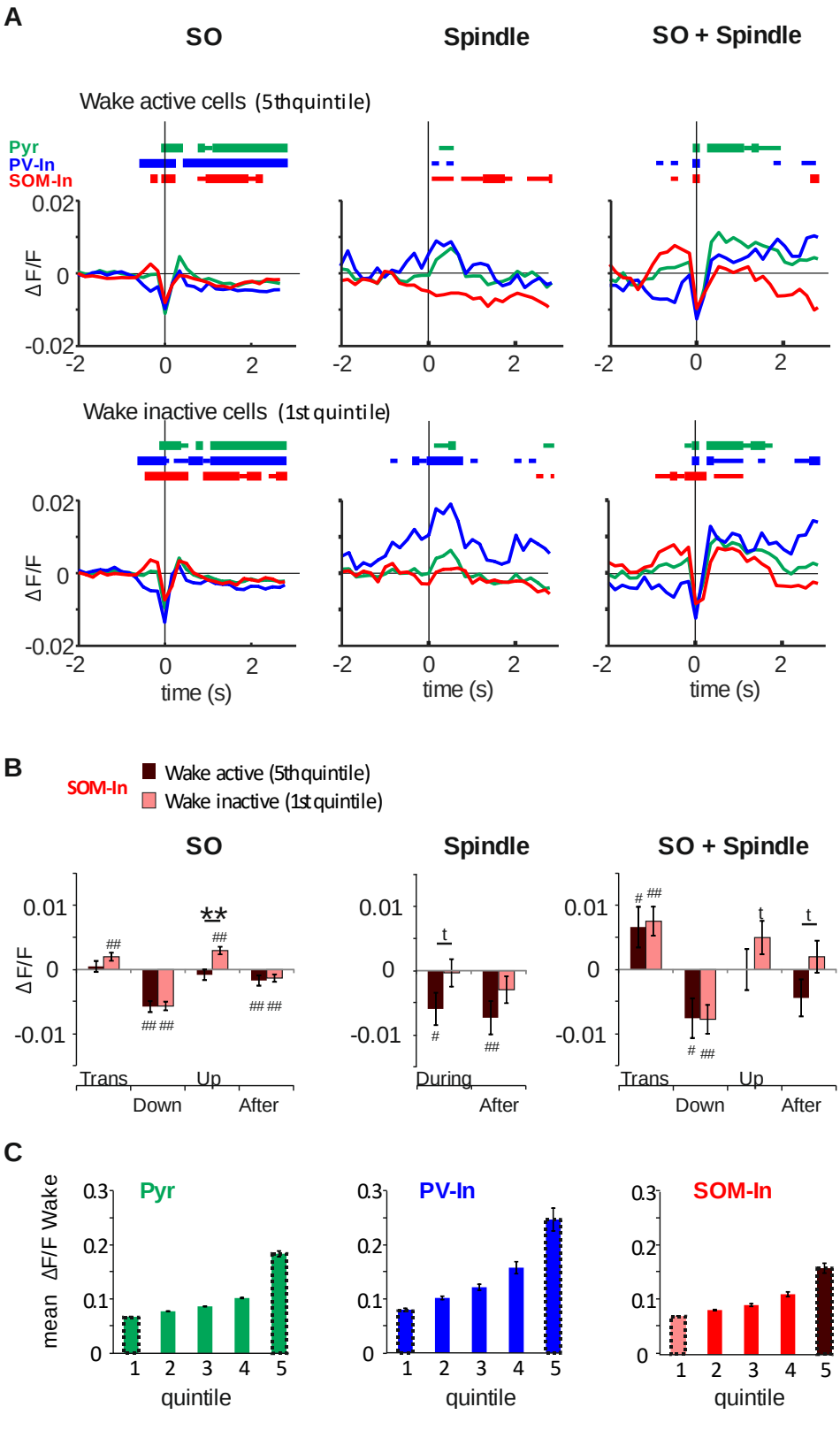
A
SO
Spindle
SO + Spindle
Wake active cells (5thquintile)
Pyr
PV-In
SOM-In
0.02
0
-0.02
ΔF/F
-2
0
2
Wake inactive cells (1st quintile)
time (s)
B
SOM-In
Wake active (5thquintile)
Wake inactive (1st quintile)
0.01
-0.01
**
##
###
t
#
Trans
Up
Down
After
During
C
mean ΔF/F Wake
Pyr
PV-In
SOM-In
0.3
0.2
0.1
1
2
3
4
5
quintile

Fig. S3. (*A*) Mean ± SEM ΔF/F signal for cell clusters of putative Pyr (green), PV-In (blue) and SOM-In (red) during slow oscillations (SO), solitary spindles (Spindle) and slow oscillations co-occurring with spindles (SO + Spindle). Signals are time locked (0 s) to the negative peak of slow oscillations (SO and SO + Spindle) or the spindle onset (Spindle). Bars on top indicate significance ($p < 0.05$) for each cell type with reference to baseline (-3 to -2 s) set to zero. Top: average traces for the 20 % cells most active during wakefulness (5th quintile) for each cell type. Bottom: average traces of the 20 % cells least active during wakefulness for each cell type (1st quintile). Average traces across all events from all animals are indicated. (*B*) Left: Comparison of mean (± SEM) ΔF/F signals between SOM-In cell cluster during solitary SO events for the positive-to-negative Transition phase (Trans, -0.32 to -0.00 s, with reference to slow oscillation negative half-wave peak = 0 s), the Down phase (-0.00 to 0.16 s), the Up phase (0.32 to 0.48 s) and the following After phase (0.54 to 3 s). Middle: Comparisons between mean (± SEM) ΔF/F signals between SOM-In cell cluster during solitary spindle events for the phase During the acute spindle (0 to 1 s with reference to spindle onset set to 0 s) and the After phase (1 to 3 s). Right: Comparison of mean (± SEM) ΔF/F signals between SOM-In cell cluster during SO + Spi events for the positive-to-negative Transition phase (Trans, -0.32 to -0.00 s, with reference to slow oscillation negative half-wave peak = 0 s), the Down phase (-0.00 to 0.16 s), the Up phase (0.32 to 0.48 s) and the following After phase (0.54 to 3 s). ** $P < 0.01$, * $P < 0.05$, t $P < 0.1$ for pairwise comparisons between solitary events and SO + Spi events respectively. ## $p < 0.01$, # $p < 0.05$, t $P < 0.1$(*C*) Mean ΔF/F ± SEM during wakefulness for quintiles of each cell type. Note highest levels for 5th quintile of PV-In.

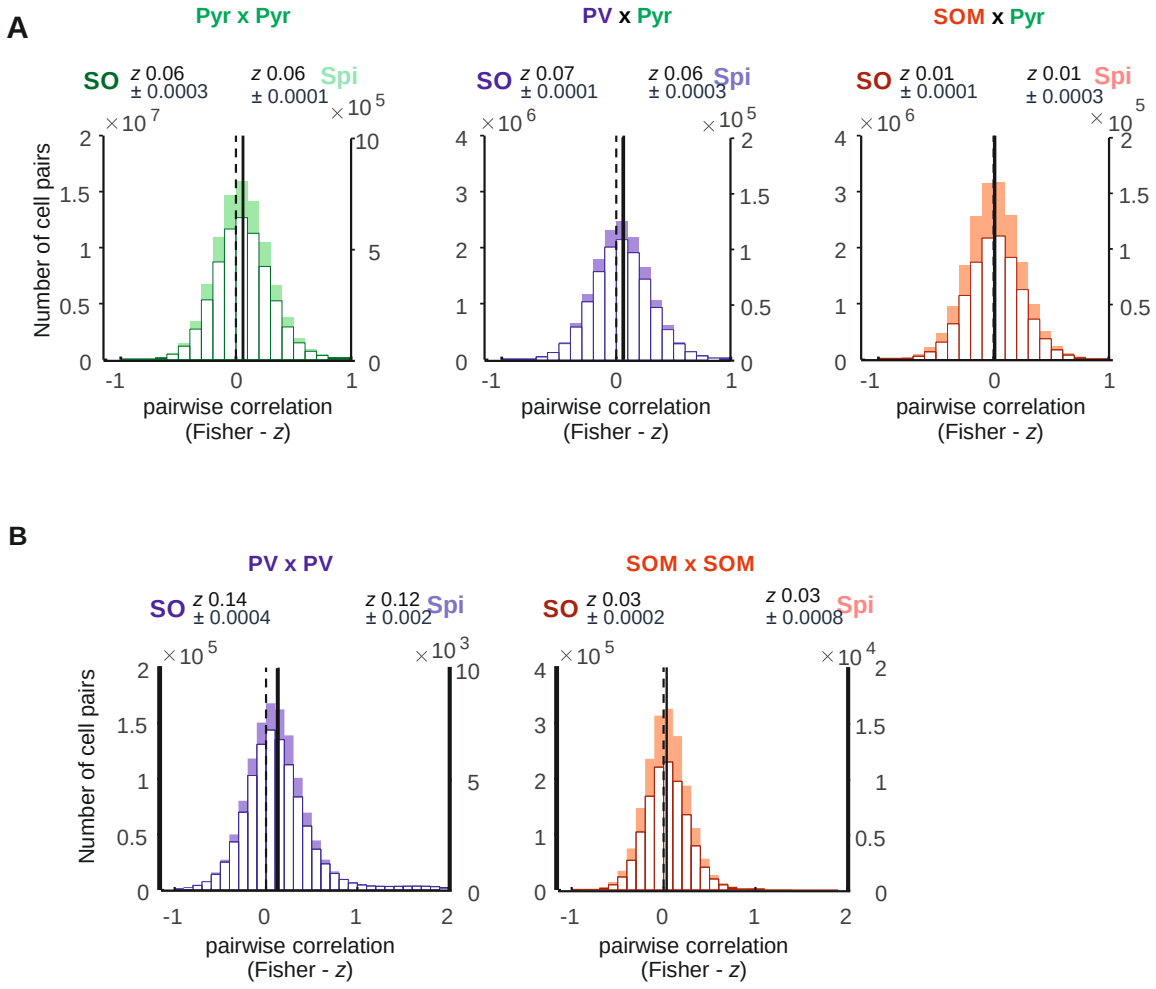

Fig. S4. Distributions of pairwise correlations in calcium activity within putative Pyr cells, PV-In, and SOM-In cells during solitary slow oscillations and spindles. Pairwise Pearson correlation of the ΔF/F signal between all cell pairs within one cell type and between all putative Pyr cells and each interneuron population were calculated during all detected solitary EEG slow oscillations and spindles (in a -2 s to +3 s-window around the slow oscillation negative half-wave peak and spindle onset). Fisher z-transformed coefficients are shown. (*A*) Distribution of correlation coefficients within the populations of putative Pyr cells (green) and between putative Pyr cells and PV-In (blue) and SOM-In (red) during solitary slow oscillations and (white) solitary spindles (colored). (*B*) Distribution of correlations within PV-In (blue) and SOM-In (red) during solitary slow oscillations (white) and solitary spindles (colored). For each distribution the mean (± SEM) is indicated). Note, distributions did not reveal distinct subgroups of highly correlated cells and none of the distributions differed significantly from normal distribution (Chi^2 –tests: all $P > 0.1$). Mean correlations, i.e., synchrony in activity for PV x Pyr and PV x PV correlations during slow oscillations was higher than during spindles. However, though significant ($P < 0.01$), effects sizes were very small (Cohen's $d < 0.1$). Note also that correlations were generally rather small, possibly reflecting that the proportion of cells actually engaging in slow oscillation and spindle events is relatively small.

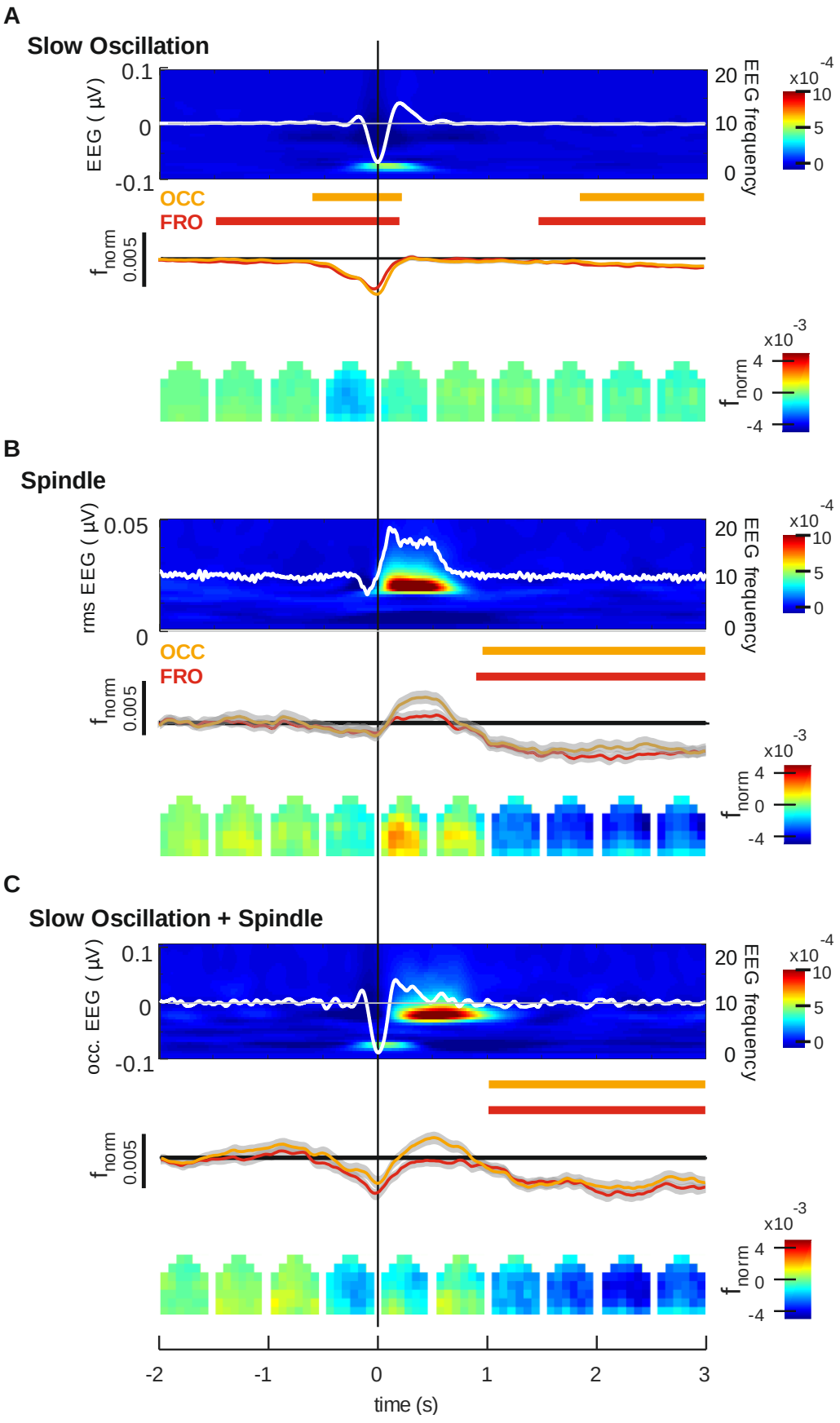
A
Slow Oscillation
EEG (µV)
0.1
0
-0.1
EEG frequency
20
10
0
x10 -4
10
5
0
OCC
FRO
f norm
0.005
x10 -3
4
0
-4
B
Spindle
rms EEG (µV)
0.05
0
C
Slow Oscillation + Spindle
occ. EEG (µV)
-2
-1
0
1
2
3
time (s)

Fig. S5. (*A*) From top to bottom: Average EEG signal (across all events from all animals) for solitary slow oscillations (from left occipital cortical recordings, white line overlaying average time-frequency plot with color-coded power) together with (middle panel) average (±SEM) calcium activity (f_{norm}) across the 4 designated anterior (red) and posterior (orange) cortical regions. Averages are time-locked to the negative half-wave peak of the slow oscillation (0 s). Intervals with significant changes in calcium activity ($p < 0.01$, relative to the baseline interval from -3 to -2 s) are indicated by red (for anterior ROIs - FRO) and orange bars (for anterior ROIs - FRO, see Figure 4 of main text for location of target ROIs). The bottom panel shows topographic changes of calcium activity in all 36 ROIs (in f_{norm}, color coded) for subsequent 500-ms time windows. Panels (*B*) and (*C*) show corresponding data for solitary spindles (Spindle) and slow oscillations co-occurring with spindles (Slow oscillation + Spindle). Note, for solitary spindles the average EEG signal (overlaying the corresponding EEG time frequency plot) shows the root mean square (RMS) amplitude, and averaging is time-locked to the spindle onset. Average traces are shown across events from 4 animals (total n = 9864, 766, 762, for solitary slow oscillations, solitary spindles, and slow oscillations co-occurring with spindles).

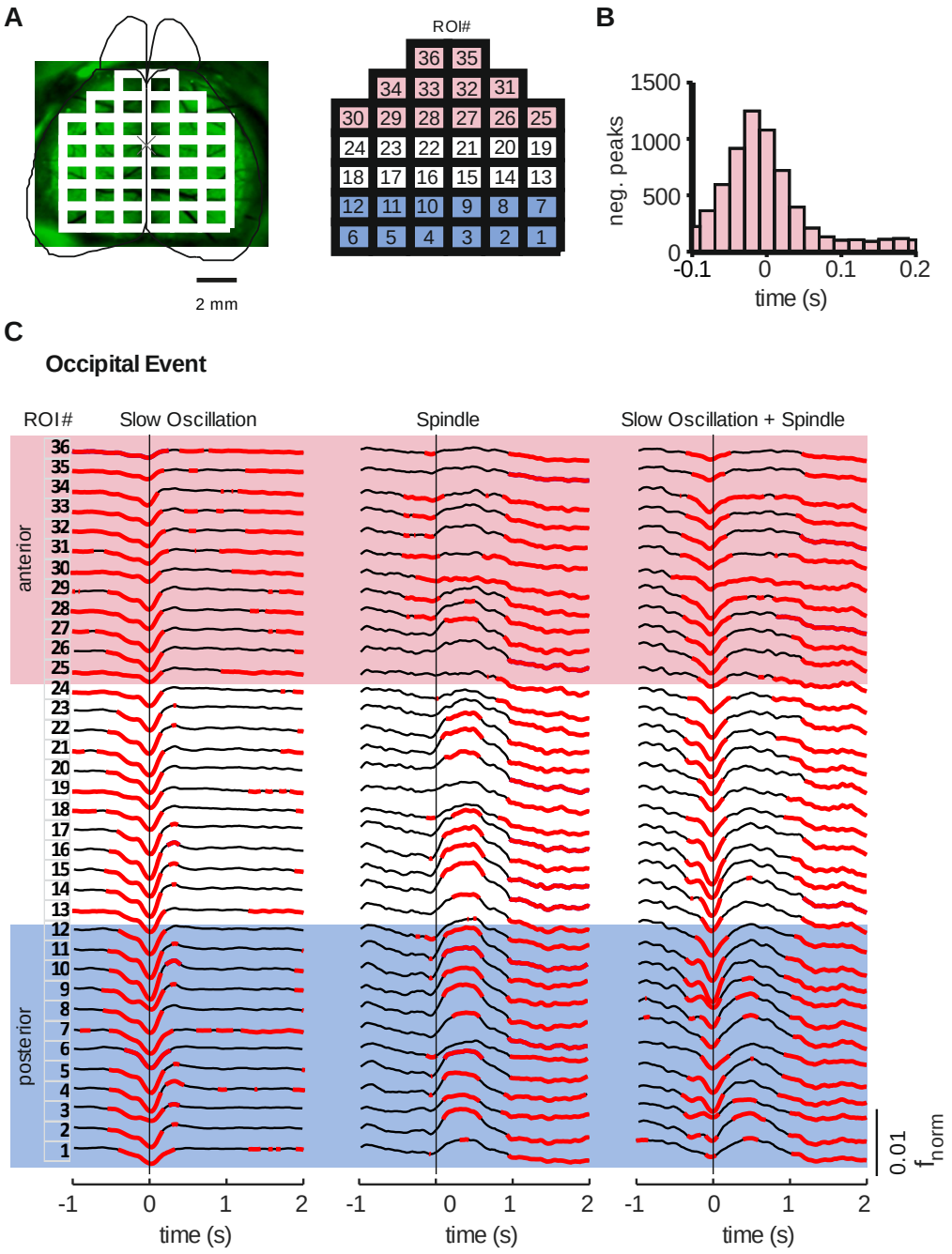

Fig. S6 (*A*) Illustration of the 36 cortical ROIs used for wide-field imaging experiments. Red-shaded area indicates anterior ROIs (#25 - #36), blue-shaded area posterior ROIs (#1 - #12). (*B*) Histogram showing the distribution of the temporal delays of slow oscillation negative half-wave peaks defined in the f_{norm} signal between frontal ROIs and occipital ROIs. Only slow oscillation events were included in this analysis, where the minimum of the f_{norm} signal was associated with the slow oscillation half-wave peak exceeding a critical threshold for both anterior and posterior regions (with the threshold defined by 0.66 standard deviations from the mean activity of the filtered 0.1 - 4 Hz signal). (*C*) Calcium activity for 36 cortical ROIs using wide-field imaging during solitary slow oscillations (left), solitary spindles (middle) and slow oscillations co-occurring with spindles (Slow oscillation + Spindle, right). Red-shaded area indicates anterior ROIs, blue-shaded area posterior ROIs. Numbering of ROIs is indicated in *A*. Average traces

across all events from 4 animals (total n = 9864, 766, 762, for solitary slow oscillations, solitary spindles, and slow oscillations co-occurring with spindles, respectively) are indicated. Averaging is time locked (0 s) to the negative half-wave peak of the slow oscillation and spindle onset, respectively. EEG events were identified in occipital EEG channel. Red marked calcium signal indicates intervals of significantly ($P < 0.05$) enhanced or reduced activity (with reference to activity during the baseline interval from -3 to -2 s).

Subject characteristics

animal #	genotype	imaging sessions	recorded Pyr	interneurons	SOs	Spindles	SOs+Spindles
1	PV-cre	1	126	17	3135	160	166
2	PV-cre	3	329	43	1272	129	52
3	PV-cre	2	241	28	3655	268	233
4	SOM-cre	3	342	45	4198	240	181
5	SOM-cre	1	123	16	596	47	32
6	SOM-cre	2	229	38	3239	215	228
7	SOM-cre	1	120	18	2836	252	200
Total:		13	1510	205	18931	1311	1092

Characteristics of EEG events

animal #	genotype	SO Duration	SO Amplitude	Spi Duration	Spi Amplitude	SO+Spi SO Duration	SOSpi SO Amplitude	SOSpi Spi
1	PV-cre	0.60 ±0.003	0.26 ±0.001	0.67 ±0.016	0.17 ±0.002	0.61 ±0.013	0.26 ±0.006	0.68
2	PV-cre	0.59 ±0.005	0.20 ±0.001	0.67 ±0.015	0.11 ±0.002	0.62 ±0.028	0.18 ±0.007	0.70
3	PV-cre	0.60 ±0.003	0.21 ±0.001	0.65 ±0.011	0.15 ±0.002	0.57 ±0.010	0.20 ±0.004	0.67
4	SOM-cre	0.64 ±0.003	0.32 ±0.001	0.67 ±0.012	0.19 ±0.002	0.64 ±0.017	0.31 ±0.007	0.72
5	SOM-cre	0.61 ±0.009	0.18 ±0.002	0.93 ±0.065	0.15 ±0.005	0.66 ±0.051	0.19 ±0.011	1.04
6	SOM-cre	0.64 ±0.004	0.25 ±0.001	0.72 ±0.015	0.15 ±0.003	0.62 ±0.013	0.25 ±0.005	0.83
7	SOM-cre	0.60 ±0.003	0.34 ±0.001	0.81 ±0.021	0.21 ±0.003	0.61 ±0.013	0.35 ±0.009	0.92

Table S1. Top - Subject characteristics: Mice and number of imaging sessions and cells imaged per animal. Bottom - Characteristics of EEG events: Mean (± SEM) duration and amplitude of slow oscillation and spindles for solitary slow oscillation (SO) and (7 - 15 Hz) spindle events and for slow oscillations co-occurring with spindles (SO + Spi).

REAGENT or RESOURCE	SOURCE	IDENTIFIER
Antibodies		
anti-PV rabbit primary antibody	Immunostar, U.S.A.,	RRID: AB_572259
anti-SOM rabbit primary antibody	Peninsula Laboratories, U.S.A.,	RRID: AB_518618
goat anti-Rabbit IgG antibody for PV conjugated with Alexa 405	Thermo Fisher Scientific	RRID: AB_221605
goat anti-Rabbit IgG antibody for SOM conjugated with Alexa 633	Thermo Fisher Scientific	RRID: AB2535732
Bacterial and Virus Strains		
AAV2/1-syn-GCaMP6f	University of Pennsylvania	Cat# CS0201
AAV2/1-flex-tdTomato	University of Pennsylvania	Cat# CS0647
AAV2/1-EF1aGFP	University of Pennsylvania	Cat# AV-1-PV1963
Experimental Models: Organisms/Strains		
Pvalb$^{tm1(cre)Arbr}$/J (PV-Cre)	Jackson	RRID: Jax: 008069
Sst$^{tm2.1(cre)Zjh}$/J (SOM-Cre)	Jackson	RRID: Jax:013044
Gt(ROSA)26Sor$^{tm95.1(CAGGCaMP6f)Hze}$/J	Jackson	RRID: Jax:024105
B6.FVB-Tg(Camk2acre)2Gsc/Cnrm Mus musculus	EMMA	RRID:IMSR_EM:01153
Software and Algorithms		
MATLAB	MathWorks	2016a & 2014b; RRID:SCR_001622
fieldtriptoolbox	www.fieldtriptoolbox.org	RRID: SCR_004849
SleepSign for Animals	Kissei Comtech, Japan	Version 3.2

Table S2. Used resources.

Movie S1. Mean f_{norm} signal of the 36 ROIs during all solitary slow oscillations. Bottom trace indicates corresponding EEG recording (speed x 0.25).

References

1. Neckelmann, D., Olsen, O.E., Fagerland, S., and Ursin, R. (1994). The reliability and functional validity of visual and semiautomatic sleep/wake scoring in the Møll-Wistar rat. Sleep *17*, 120–131.

2. Oyanedel, C.N., Kelemen, E., Scheller, J., Born, J., and Rose-John, S. (2015). Peripheral and central blockade of interleukin-6 trans-signaling differentially affects sleep architecture. Brain. Behav. Immun. *50*, 178–185.

3. David, F., Schmiedt, J.T., Taylor, H.L., Orban, G., Di Giovanni, G., Uebele, V.N., Renger, J.J., Lambert, R.C., Leresche, N., and Crunelli, V. (2013). Essential thalamic contribution to slow waves of natural sleep. J. Neurosci. *33*, 19599–19610.

4. Mölle, M., and Born, J. (2011). Slow oscillations orchestrating fast oscillations and memory consolidation. Progr. Brain Res. *193*, 93–110.

5. Mölle, M., Eschenko, O., Gais, S., Sara, S.J., and Born, J. (2009). The influence of learning on sleep slow oscillations and associated spindles and ripples in humans and rats. Eur. J. Neurosci. *29*, 1071–1081.

6. Mölle, M., Bergmann, T., Marshall, L., and Born, J. (2011). Fast and slow spindles during the sleep slow oscillation: disparate coalescence and engagement in memory processing. Sleep *34*, 1411–1421.

7. Eschenko, O., Ramadan, W., Molle, M., Born, J., and Sara, S.J. (2008). Sustained increase in hippocampal sharp wave ripple activity during SWS after learning. Learn. Mem. *15*, 222–228.

8. Mölle, M., Marshall, L., Gais, S., and Born, J. (2002). Grouping of spindle activity during slow oscillations in human non-rapid eye movement sleep. J. Neurosci. *22*, 10941–10947.

9. English, D.F., Peyrache, A., Stark, E., Roux, L., Vallentin, D., Long, M. A., and Buzsáki, G. (2014). Excitation and inhibition compete to control spiking during hippocampal ripples: Intracellular study in behaving mice. J. Neurosci. *34*, 16509–16517.

10. Niethard, N., Hasegawa, M., Itokazu, T., Oyanedel, C.N., Born, J., and Sato, T.R. (2016). Sleep-stage-specific regulation of cortical excitation and inhibition. Curr. Biol. *26*, 2739–2749.

11. Pologruto, T. A., Sabatini, B.L., and Svoboda, K. (2003). ScanImage: flexible software for operating laser scanning microscopes. Biomed. Eng. Online *2*, 13.